REPORT

Aberrant cytoplasmic intron retention is a blueprint for RNA binding protein mislocalization in amyotrophic lateral sclerosis

Giulia E. Tyzack,[1,2,†] Jacob Neeves,[1,2,†] Hamish Crerar,[1,2] Pierre Klein,[1,2] Oliver Ziff,[1,2] Doaa M. Taha,[1,2,3] Raphaëlle Luisier,[4,‡] Nicholas M Luscombe[1,5,6,‡] and Rickie Patani[1,2,‡]

[†,‡]**These authors contributed equally to this work.**

Abstract

We recently described aberrantly increased cytoplasmic SFPQ intron-retaining transcripts (IRTs) and concurrent SFPQ protein mislocalization as new hallmarks of amyotrophic lateral sclerosis (ALS). However the generalizability and potential roles of cytoplasmic IRTs in health and disease remain unclear. Here, using time-resolved deep-sequencing of nuclear and cytoplasmic fractions of hiPSCs undergoing motor neurogenesis, we reveal that ALS-causing VCP gene mutations lead to compartment-specific aberrant accumulation of IRTs. Specifically, we identify >100 IRTs with increased cytoplasmic abundance in ALS samples. Furthermore, these aberrant cytoplasmic IRTs possess sequence-specific attributes and differential predicted binding affinity to RNA binding proteins (RBPs). Remarkably, TDP-43, SFPQ and FUS - RBPs known for nuclear-to-cytoplasmic mislocalization in ALS - abundantly and specifically bind to this aberrant cytoplasmic pool of IRTs, as opposed to any individual IRT. Our data are therefore consistent with a novel role for cytoplasmic IRTs in regulating compartment-specific protein abundance. This study provides new molecular insight into potential pathomechanisms underlying ALS and highlights aberrant cytoplasmic IRTs as potential therapeutic targets.

1 The Francis Crick Institute, 1 Midland Road, London NW1 1AT, UK

2 Department of Molecular Neuroscience, UCL Institute of Neurology, Queen Square, London, UK

3 Zoology Department, Faculty of Science, Alexandria University, Alexandria 21511, Egypt

4 Idiap Research Institute, Martigny, Switzerland

5 UCL Genetics Institute, University College London, Gower Street, London WC1E 6BT, UK

6 Okinawa Institute of Science and Technology Graduate University, Okinawa 904-0495, Japan

Correspondence to: Raphaëlle Luisier

Idiap Research Institute, Martigny, Switzerland

E-mail: raphaelle.luisier@idiap.ch

Correspondence may also be addressed to: Rickie Patani

The Francis Crick Institute, 1 Midland Road, London NW1 1AT, UK

E-mail: rickie.patani@ucl.ac.uk

Running title: Cytoplasmic intron retention in VCP-ALS

Keywords: Cytoplasmic intron retention; human stem cell model; nuclear/cytoplasmic fractionation; amyotrophic lateral sclerosis; protein mislocalization

Studies have demonstrated that intron retention (IR) is more frequent in mammals than originally recognized, affecting transcripts from a majority of genes (Yap *et al.*, 2012*a*, Braunschweig *et al.*, 2014*a*; Boutz *et al.*, 2015; Mauger *et al.*, 2016). It is noteworthy that neural cells, with their exceptional polarity and compartmentalisation, exhibit higher degrees of IR compared with other cell types (Yap *et al.*, 2012*a*, Braunschweig *et al.*, 2014*a*; Mauger *et al.*, 2016). Indeed, IR is a prominent mode of splicing during early neuronal differentiation (Braunschweig *et al.*, 2014*a*; Luisier *et al.*, 2018) and plays a functional role in neuronal homeostasis (Buckley *et al.*, 2011, Yap *et al.*, 2012*b*, Braunschweig *et al.*, 2014*b*; Mauger *et al.*, 2016). IR has previously been implicated in regulating the transcriptome by coupling to RNA degradation pathways (Yap *et al.*, 2012*a*; Colak *et al.*, 2013; Wong *et al.*, 2013, Braunschweig *et al.*, 2014*a*; Kilchert *et al.*, 2015). Although intron-retaining transcripts (IRTs)

have predominantly been identified as residing within the nucleus where they are degraded (Yap *et al.*, 2012*b*, Braunschweig *et al.*, 2014*b*; Boutz *et al.*, 2015), there is an expanding body of evidence demonstrating the cytoplasmic localisation of stable IRTs (Buckley *et al.*, 2011; Khaladkar *et al.*, 2013; Sharangdhar *et al.*, 2017; Saini *et al.*, 2019; Price *et al.*, 2020). However, their prevalence and role remain understudied. One of the few studies focusing on a cytoplasmic IRT showed that a retained intron in the *Calm3* transcript determined its dendritic localization (Sharangdhar *et al.*, 2017), thus revealing an addressing (or 'zip-coding') function of cytoplasmic IR. This study raises the possibility of new roles for intronic RNA sequences beyond a nuclear function, and suggests that cytoplasmic IR programmes are relevant to human neurological function and their perturbation, therefore, to disease.

Amyotrophic lateral sclerosis (ALS) is a rapidly progressive and incurable adult-onset condition, which leads to the relatively selective degeneration of motor neurons (MNs). The molecular pathological hallmark of ALS is the nuclear-to-cytoplasmic mislocalization of key RNA binding proteins (RBPs) (Neumann *et al.*, 2006; Luisier *et al.*, 2018; Tyzack *et al.*, 2019), although the underlying mechanism remains elusive. ALS-causing gene mutations implicate crucial regulators of RNA-processing, which are normally expressed throughout development (Sreedharan *et al.*, 2008; Vance *et al.*, 2009). This raises the hypothesis that post-transcriptional changes, including those occurring during neurodevelopment, may play a pivotal role in the underlying molecular pathogenesis of ALS. We recently described IR as the predominant splicing event characterizing early stages of motor neuron lineage restriction from human iPSCs, which is perturbed by genetically diverse ALS-causing mutations (Luisier *et al.*, 2018). However, whether this process affects the nuclear or cytoplasmic subcellular compartments similarly remains unresolved. Few studies have examined compartment-specific IR in differentiated neurons (Buckley *et al.*, 2011; Price *et al.*, 2020), and to our knowledge, no study has comprehensively investigated cytoplasmic IR programmes during human motor neurogenesis, nor systematically characterized the effect of an ALS-causing mutation.

Here, we combine cellular fractionation of hiPSCs undergoing motor neurogenesis with deep RNA-sequencing (RNA-seq) of approximately 100 million paired end reads per sample to gain insights into the molecular 'logic' governing IR programmes in healthy and disease states. This is a rich resource for researchers across the disciplines of basic and applied neuroscience, constituting six timepoints during motor neurogenesis for four control lines (from 4 healthy individuals) and three ALS lines (from 2 patients carrying mutations in the VCP gene), which have been separated into nuclear and cytoplasmic fractions. Indeed, this resource allowed us to

make important insights into the nature of aberrant IR in a human stem cell model of ALS. Specifically, we provide a taxonomy for aberrant IR based on nucleocytoplasmic distribution, *cis* attributes and predicted intron binding affinities to major RBPs. Remarkably, this revealed >100 IRT species in the cytoplasm of ALS cultures, suggesting that this is a more widespread phenomenon than previously recognized. Furthermore we confirm direct binding of Splicing Factor Proline And Glutamine Rich (SFPQ) protein with SFPQ IRT within the cytoplasm of our hiPSC ALS model along with preliminary evidence of a functional interaction between them. In summary, we have uncovered a novel class of cytoplasmic IRTs that exhibits predictive value for the nuclear-to-cytoplasmic mislocalization of key RBPs, which constitutes a recognized molecular hallmark of ALS.

METHODS

Detailed methods are provided in the Supplementary material.

Ethics Statement

Informed consent was obtained from all patients and healthy controls in this study. Experimental protocols were all carried out according to approved regulations and guidelines by UCLH's National Hospital for Neurology and Neurosurgery and UCL's Institute of Neurology joint research ethics committee (09/0272).

Cell Culture

Human induced pluripotent stem cells (hiPSCs) were maintained on Geltrex (Life Technologies) with Essential 8 Medium media (Life Technologies), and passaged using EDTA (Life Technologies, 0.5 mM). All cell cultures were maintained at 37°C and 5% carbon dioxide. Directed differentiation of hiPSCs to motor neurons was performed as previously described (Hall *et al.*, 2017). Details of the lines used in this study are provided in **Supplementary Table 1**. One of the control lines used (control 3) is commercially available and was purchased fromThermoFisher Scientific (cat. number A18945).

Data availability

All sequence data for this project has been deposited at NCBI GEO database under accession

number **GSE152983**. Additional data supporting the findings of this study are available from the corresponding authors, upon reasonable request.

RESULTS

High coverage RNA-seq data from nuclear and cytoplasmic fractions during human motor neurogenesis

We analysed high-throughput poly(A) RNA-seq data derived from nuclear and cytoplasmic fractions of human induced pluripotent stem cells (hiPSC; day 0), neural precursors (NPC; day 3 and day 7), 'patterned' precursor motor neurons (ventral spinal cord; pMN; day 14), post-mitotic but electrophysiologically immature motor neurons (MN; day 22), and electrophysiologically active MNs (mMNs; day 35). The cellular material was derived from four healthy controls and two ALS patients with Valosin Containing Protein (VCP) mutations: R155C and R191Q, hereafter termed VCP^{mu} (**Fig. 1A;** 95 samples from 6 time-points and 2 genotypes (healthy and VCP^{mu} related ALS); 4 clones from 4 different healthy controls and 3 clones from 2 VCP^{mu} patients). Further details of the samples sequenced can be found in **Table S1** and details of the RNAseq quality control in **Table S2**. Cells from each stage of differentiation were characterised as previously reported (Hall *et al.*, 2017). The efficiency of cellular fractionation was assessed both at protein and RNA level. The predominantly nuclear proteins histone H3 and PSPC1 were highly enriched in the nuclear fraction, whereas the cytosolic enzyme GAPDH was mainly detected in the cytoplasm (**Fig. 1B)**. Similarly, the presence of *GAPDH* intronic RNA was negligible in the cytoplasm, suggesting that leakage of RNA from the nucleus to the cytoplasm due to the fractionation protocol was minimal. Importantly, the efficiency of fractionation was comparable between control and VCP^{mu} lines. Singular value decomposition analysis of 18,834 reliably expressed genes across the 95 samples revealed that developmental stage and cellular fractions were the largest contributors to transcriptome diversity, explaining 41% and 15% of the variance, respectively. Notably the VCP^{mu} does not affect these processes and samples cluster with their age- and fraction-matched control counterparts (**Figs. 1C-E**). Unsupervised hierarchical clustering (Spearman rank correlation and complete-linkage clustering) of the 95 samples using 18,834 genes segregated samples by developmental stage rather than genetic background (**Supplementary Fig. S1A**).

Widespread aberrant cytoplasmic IR in a human stem cell model of ALS

We previously identified ALS-related aberrant cytoplasmic SFPQ IRT and concurrent SFPQ protein mislocalization (Luisier *et al.*, 2018). Here we tested whether aberrant cytoplasmic IR is a generalizable transcriptomic phenomenon in ALS. We examined patterns of splicing using the RNA-seq pipeline VAST-TOOLS (Irimia *et al.*, 2014). In line with our previous study, increased intron retention is the dominant feature of the splicing program during early neural differentiation in both the nucleus and the cytoplasm (**Supplementary Figs. S1B-E**). We identified 791 nuclear (527 included and 264 skipped) and 329 cytoplasmic (204 included and 125 skipped) alternative splicing events that are statistically significantly different between VCP^{mu} and control samples in at least one time-point (**Supplementary Fig. 1F,G**). In line with our previous study, the majority of inclusion events between VCP^{mu} and control samples were retained introns (**Fig. 1F, *upper***). We find that these events peak in pMNs (day 14 *in vitro*) (**Fig. 1F, *lower***) when we observe a coincident decrease in expression of splicing factors (**Fig. 1G** and **Supplementary Fig. S1H**); most notable are the 112 aberrant IR events in the cytoplasmic fraction. Given that most VCP-driven aberrant retained introns events peak at day 14, we subsequently chose to focus on this time-point in the following analysis. Collectively, these findings demonstrate that aberrant cytoplasmic IR is a widespread phenomenon in ALS that occurs at an early stage during motor neurogenesis.

A nucleocytoplasmic taxonomy for aberrant IRTs

We next manually curated the list of nuclear and cytoplasmic VCP-mutation related aberrant IR events, focusing on pMNs (day 14 in vitro, DIV=14). We identified three categories of aberrant IRTs in VCP^{mu} : 1) 237 predominantly in the nucleus; 2) 63 in both the nucleus and the cytoplasm; 3) 49 predominantly in the cytoplasm (**Fig. 2A, Tables** S3-S5). Gene Ontology functional enrichment analysis shows the specific biological association of affected genes, including cell cycle for the predominantly nuclear IRTs and protein localisation for those that are predominantly cytoplasmic (**Fig. 2B**). To address whether these IRTs exist in MNs carrying other ALS causing mutations, including in FUS and SOD1 mutant MNs, we probed external whole-cell RNAseq datasets and confirmed the presence of aberrant IRTs in these two genetically diverse forms of ALS. Notably the SOD1 data are derived from isogenic pairs and further allows us to confirm that the IRTs observed are mutation-dependent. We find that although our high-confidence set of 349 aberrant IRTs are also generally affected in FUS and SOD1 mutant motor neurons, the pool of 49 IRTs that is predominantly affected in the cytoplasm of VCP mutants exhibits the strongest effect in both FUS and SOD1 mutant motor

neurons (**Figs. 2C,D)**. Next, looking at the cytoplasmic abundance of the IRTs relative to the spliced transcripts, we find that the IRTs account for ~40% of the absolute amount of transcripts in the cytoplasm of VCP mutant cultures compared to ~20% in the cytoplasm of control samples. This result indicates that the cytoplasmic IRTs abound in our iPSC model and are significantly increased by ALS-causing VCP mutations (**Supplementary Fig. 2A)**. We previously identified aberrant IR in SFPQ in VCP^{mu} at an early stage of MN development (Luisier *et al.*, 2018), which we validated here again by RNAseq and RT-PCR (**Figs. 2E,F; Supplementary Fig. 2B**). Importantly, we validated 3 further IRTs (*OGT*, *TUSC3*, and *DDX39*) using RT-PCR, where we not only confirmed the increase in intron retention ratio (**Supplementary Fig. 2C**), but also demonstrated an increase in cytoplasmic abundance of these IRTs (**Fig. 2G** and **Supplementary Figs. 2D-E**). This finding was present when normalising using either cell compartment specific or whole cell housekeeping genes (**Figs. 2F,G** and **Supplementary Figs. 2C-E**, respectively). The finding that a large number of IRTs, including *SFPQ*, *OGT*, *TUSC3*, and *DDX39*, exhibit a specific increase in cytoplasmic abundance in VCP^{mu} cultures suggests that VCP mutation leads to aberrant nuclear export and/or cytoplasmic stabilisation of a specific class of IRTs underlying stereotyped cellular dysfunction as a consequence.

Aberrant predominantly cytoplasmic IRTs abundantly bind RBPs

Prior studies have shown that retained introns are on average shorter and more G/C rich (Galante *et al.*, 2004; Sakabe and de Souza, 2007, Braunschweig *et al.*, 2014*a*). Strikingly, here we find that only the predominantly nuclear aberrantly retained introns exhibit these features. In complete contrast, aberrantly retained introns within the cytoplasm (including both those present within the nucleus and cytoplasm, and those in the cytoplasm predominantly) are on average longer and have lower GC content (**Figs. 3A,B**). Furthermore, the predominantly nuclear aberrant IRTs correlate with a cytoplasmic decrease in gene expression of their non-intron-retaining counterparts: this is consistent with prior observations showing that nuclearly-detained IRTs reduce the level of gene expression (Braunschweig *et al.*, 2014*a*). Conversely, IRTs found in the cytoplasm correlate with increased gene expression within the nucleus (**Supplementary Fig. 2F).** Importantly this suggests that previously reported features (Galante *et al.*, 2004; Sakabe and de Souza, 2007, Braunschweig *et al.*, 2014*a*) discriminate nuclearly detained IRTs from cytoplasmic ones. Two additional features further discriminate cytoplasmic-predominant events from those found in both compartments: 1) a high

conservation score (**Fig. 3C**) and 2) a greater abundance of RBP crosslinking events in the cytoplasmic only retained introns (Sloan *et al.*, 2016; Van Nostrand *et al.*, 2017) (**Fig. 3D**).

Aberrant cytoplasmic IRTs are a blueprint for RBP mislocalization in VCP-related ALS

The finding that cytoplasmic aberrant IRTs abundantly bind to RBPs raises the hypothesis that this interaction drives hallmark RBP mislocalization events in ALS. Indeed we previously reported that the *SFPQ* IRT and the SFPQ protein itself, which are predicted to avidly bind to each other, are both exported to the cytoplasm thus providing a potential mechanism for SFPQ mislocalization in ALS (Luisier *et al.*, 2018). We therefore further examined the nature of the interaction between RBPs and aberrant cytoplasmic IRTs using our richer dataset. At least 27 RBPs systematically exhibit statistically significant increased binding to cytoplasmic-predominant retained introns compared with their nuclear-predominant counterparts (**Fig. 3E**). These RBPs form a densely connected network of experimentally validated interacting proteins that are enriched in mRNA metabolism functions (**Fig. 3F**). The network includes a subset of 9 RBPs with known functions in processing capped intron-containing pre-mRNA, which further implicates disrupted post-transcriptional splicing in ALS pathogenesis. Importantly, also within this network of RBPs are those that exhibit hallmark nuclear-to-cytoplasmic mislocalization in ALS: SFPQ (**Fig. 3G**), Trans-activation Response DNA Binding Protein (TDP-43) TDP-43, and FUS (**Supplementary Fig. 2H)** (Neumann *et al.*, 2006; Luisier *et al.*, 2018; Tyzack *et al.*, 2019).

Notably, we have previously demonstrated reduced nuclear to cytoplasmic ratio of SFPQ, FUS and TDP-43 proteins in VCP mutant hiPSC-derived neural precursors and/or motor neurons (Hall *et al.*, 2017; Luisier *et al.*, 2018; Tyzack *et al.*, 2019; Harley and Patani, 2020; Harley *et al.*, 2020). In order to contextualize these previous protein mislocalization findings with our current study, we next sought to examine the mechanistic relationship between RBP function and aberrant accumulation of IRTs in the cytoplasm, focusing on the interaction between SFPQ protein and *SFPQ* IRTs. We first performed RNA immunoprecipitation (RIP) to demonstrate that the SFPQ protein physically interacts with SFPQ IRT (**Fig. 3H** and **Supplementary Fig. 3A**). When considered together with the fact that we also find a higher abundance of SFPQ IRT in the input from the VCP mutant when compared to input from the control or the spliced/constitutive transcripts in either genotype (**Fig. 3I**), these data are consistent with an increased specific interaction between SFPQ IRT and SFPQ protein in VCP mutant cultures compared to control counterparts.

We next knocked down SFPQ protein using an siRNA approach (**Supplementary Fig. 3B-C**). We found that while this siRNA-mediated knockdown resulted in a substantial reduction in expression of both SFPQ spliced transcript and SFPQ IRT (**Supplementary Figs. 3B, D and E**), a significant increase in the SFPQ intron retention ratio relative to the spliced transcript was observed (**Supplementary Fig. 3F**). This result suggests that SFPQ protein autoregulates its own intron retention, which is consistent with a recent study reporting significant retention of long intron upon SFPQ depletion (Stagsted *et al.*, n.d.; Pervouchine *et al.*, 2019). Altogether our data lend support to a model whereby ALS leads to an increase in the abundance of a class of cytoplasmic IRTs with a large capacity for binding RBPs. In turn, this may create an environment that encourages nuclear-to-cytoplasmic mislocalization of their IRT-bound RBPs followed by nuclear loss of function and/or cytoplasmic gain of function (**Fig. 4**).

DISCUSSION

Recent studies have demonstrated that IR is more frequent in mammals than previously recognized (Yap *et al.*, 2012*a*, Braunschweig *et al.*, 2014*a*; Boutz *et al.*, 2015; Mauger *et al.*, 2016). We previously identified aberrant cytoplasmic IR in the SFPQ transcript across human stem cell models of diverse genetic forms of ALS (including those caused by mutations in VCP, SOD1 and FUS genes) (Luisier *et al.*, 2018). In the present study, we sought to understand the generalizability of cytoplasmically localised aberrant IRTs in ALS by combining directed differentiation of patient-specific hiPSCs into spinal MNs with cellular fractionation and deep (polyA) RNA sequencing. We showed that aberrant cytoplasmic IR is indeed a widespread molecular phenomenon in ALS that comprises at least 112 transcripts including SFPQ. Furthermore we specifically demonstrated an increase in the cytoplasmic abundance of the intronic sequences, suggesting aberrant nuclear export and/or cytoplasmic stabilisation of a specific pool of IRTs in VCP mutant samples. Importantly, a significant overlap of these aberrant events have been previously recapitulated in RNAseq data sets from terminally differentiated motor neurons carrying mutations in SOD1 or FUS genes (Kiskinis *et al.*, 2014; Kapeli *et al.*, 2016). Furthermore, the most significant intron retention event identified in our aforementioned study, intron 9 of the SFPQ transcript, has been recently reproduced in human post mortem tissue from sporadic ALS cases, demonstrating the predictive power of our hiPSC model (Hogan *et al.*, n.d.).

To better understand the nature of cytoplasmic IRTs, we categorized the aberrant IR events into three classes according to their nucleocytoplasmic distribution (predominantly nuclear, predominantly cytoplasmic and those present in both compartments). We chose to direct our attention to day 14 of our motor neurogenesis protocol as this was where the majority of aberrant intron retention events were observed. Retained introns during neurogenesis have previously been shown to exhibit a highly correlated set of *cis* features comprising an ‘‘IR code’’ that can reliably discriminate retained from constitutively spliced introns (Braunschweig *et al.*, 2014*a*). Examining the cis attributes of the three categories of IRTs, we found that aberrantly retained introns that are predominantly in the nucleus of VCP mutant cultures display similar lengths and GC content to this ‘IR code’ (Braunschweig *et al.*, 2014*a*). IR has been previously implicated in fine-tuning the cellular transcriptome by targeting transcripts to RNA degradation pathways such as nonsense mediated decay (Yap *et al.*, 2012*a*; Colak *et al.*, 2013; Wong *et al.*, 2013, Braunschweig *et al.*, 2014*a*; Kilchert *et al.*, 2015). The retained introns characterised in the aforementioned studies act broadly to reduce the levels of transcripts that are not required (Boutz *et al.*, 2015; Braun *et al.*, 2017). Indeed, the category of predominantly nuclear aberrant IRTs also correlates with reduced gene expression in our data. Remarkably, however, the two other categories we identified exhibit an almost opposite effect on their gene expression levels and thus stimulated further investigation. Our study further revealed a specific class of cytoplasmic IRTs that 1) have unique features compared to those reported in previous studies and 2) have conspicuously high affinity for RBPs, including those that are mislocalized in ALS (TDP43, FUS and SFPQ) (Neumann *et al.*, 2006; Luisier *et al.*, 2018; Tyzack *et al.*, 2019). These findings raise the hypothesis that a subset of cytoplasmic IRTs have a distinct role compared to the previously reported IRTs that regulate gene expression and translation through coupling with nonsense mediated decay (NMD) (Braunschweig *et al.*, 2014*a*).

RNA localization to distinct subcellular compartments has been shown to regulate spatio-temporal control of protein expression (Holt and Bullock, 2009) but less is known about their role in protein localisation. Here we demonstrate for the first time a direct interaction between SFPQ protein and *SFPQ* IRT in the cytoplasm and further show siRNA SFPQ knockdown related increase in SFPQ IR. These data support a model where nuclear SFPQ binding to its retained intron facilitates splicing under normal circumstances which is consistent with a recent study showing significant retention of long introns upon SFPQ depletion (Stagsted et al., n.d.). An increase in *SFPQ* IRT cytoplasmic abundance may then lead to SFPQ

nuclear-to-cytoplasmic mislocalisation, SFPQ nuclear loss of function and consequently aberrant splicing of SFPQ intron 9, which in turn exacerbates SFPQ nuclear loss of function. However, we have not formally excluded the possibility that an increase in SFPQ IRT upon knockdown is caused by differential accessibility or targeting of the SFPQ IRTs by the siRNAs. Therefore, future experiments should further address the specific role of nuclear SFPQ protein in regulating retention of intron 9 within its own transcript. Altogether we propose that a subset of IRTs aberrantly accumulate in the cytoplasm and their intronic sequences serve as 'blueprints' for the hallmark protein mislocalization events in ALS by creating a mislocalization-prone environment for their bound (and usually predominantly nuclear) RBPs (**Fig. 4**). This is reinforced by the fact that the RBPs with the largest difference in binding affinity between the predominantly cytoplasmic vs predominantly nuclear aberrant IR are those known to be mislocalized in ALS: TDP-43, FUS and SFPQ. However, further work is needed to definitively resolve the nature of the interaction between cytoplasmically mislocalized RBPs and cytoplasmic IRTs.

The first systematic characterization of IR during neuronal lineage restriction examined time-resolved RNAseq data during the differentiation of cortical glutamatergic neurons from murine embryonic stem (ES) cells. This study established that IR progressively increases during neuronal differentiation and down-regulates non-physiologically relevant transcripts (Braunschweig *et al.*, 2014*a*). Drawing on RNAseq data from our established hiPSC model (Hall *et al.*, 2017), we subsequently reported a transient developmental IR programme early during neurogenesis from human pluripotent stem cells (Luisier *et al.*, 2018). It is noteworthy that the majority of studies have focused on nuclear IRTs and that the importance of cytoplasmic IRTs remains relatively understudied, particularly in the contexts of neuronal development and disease. In the present study we show that a large proportion of the transcripts exhibiting transient IR during neuronal development are indeed not restricted to the nucleus but transiently localise to the cytoplasm, and that this pool has strong binding affinity for RBPs. Based on these findings we hypothesise that a subset of neurodevelopmentally-regulated IRTs is specifically targeted to the cytoplasm where they attract RBPs through direct interaction leading to a transient decrease in splicing machinery in the nucleus. The cytoplasmic relocalisation of splicing factors might lead to the transient down-regulation of splicing machinery as previously reported (Luisier *et al.*, 2018). This adds a new and interesting complexity to the potential roles of IRTs, including in regulating gene expression during neuronal development (Braunschweig et al. 2014). Future studies will directly assess this

hypothesis. In summary, we propose that cytoplasmic retained introns function as RNA regulators in the homeostatic control of RBP localisation and that an ALS-related aberrant increase in cytoplasmic IR transcripts disrupts this process.

FIGURES

Figure 1 Time-resolved cellular fractionation and RNA-sequencing during human motor neurogenesis reveals widespread aberrant cytoplasmic IR in ALS. A. Schematic depicting the iPSC differentiation strategy for motor neurogenesis. Arrows indicate sampling time-points in days when cells were fractionated into nuclear and cytoplasmic compartments prior to deep (polyA) RNA-sequencing. Four iPSC clones were obtained from four different healthy controls and three iPSC clones from two ALS patients with VCP mutations: R155C and R191Q; hereafter termed VCP^{mu}. Induced-pluripotent stem cells (iPSC); neural precursors (NPC); "patterned" precursor motor neurons (ventral spinal cord; pMN); post-mitotic but electrophysiologically inactive motor neurons (MN); electrophysiologically active MNs (mMN). **B.** Representative QC data for fractionation of samples at DIV=14 at protein level (Western blot, top) and RNA level (qPCR, bottom). In the Western blot, histone H3 and PSPC1 were chosen as protein markers for the nuclear faction, and GAPDH was used as cytosolic marker. In the qPCR, the ratio between intronic and exonic GAPDH sequences was measured in both fractions to exclude the leakage of nuclear RNA into the cytosolic fraction due to disruption of nuclei during the fractionation. Data is expressed as mean±SD from four lines per group. **C.** SVD performed on normalized 18,834 gene expression values across 95 samples. Samples are plotted by their coordinates along PC1 (41% of variance) and PC2 (15% of variance). Colors of data points indicate similar time in culture: iPSC (dark blue), DIV=3 (blue; NPC1), DIV=7 (light blue; NPC2), DIV=14 (grey; pMN), DIV=22 (lightgreen; MN) and DIV=35 (dark green; eMN). **D.** Same as (**C**) with colors of data points indicating similar cellular fractions: nuclear fraction (gold) and cytoplasmic fraction (blue). **E.** Same as (**C**) with colors of data points indicating either control samples (red) or VCP^{mu} samples (blue). **F.** (*upper*) Pie charts representing proportions of included splicing events in VCP^{mu} at all timepoints of motor neurogenesis compared with age-matched control samples in nuclear (upper chart) and cytoplasmic (lower chart) fractions. Total number of events are indicated above the chart. Intron retention (IR); alternative exon (AltEx); microexons (MIC); alternative 5′ and 3′ UTR (Alt5 and Alt3). (*lower*) Bar graphs representing the number of retained introns

in VCP^{mu} compared to control samples at specific timepoints during MN differentiation. Nuclear fraction (gold; left). Cytoplasmic fraction (blue; right). **G.** Boxplots showing the distributions of cytoplasmic log2 fold-changes for 72 essential splicing factor genes (**Table S9**) between VCP^{mu} and controls.

Figure 2 Aberrant nuclear and cytoplasmic intronic sequences exhibit distinct characteristics. A. Schematic of our proposed taxonomy for aberrant IRTs (left) and bar graphs (right) representing the numbers of retained introns in VCP^{mu} compared to control samples at DIV=14 that are predominantly nuclear (gold bar), aberrant in both nucleus and cytoplasm (grey bar), or predominant in cytoplasm (blue bar). The number of events in each category is indicated above the bar. **B.** Bar plots displaying the enrichment scores for GO biological functions of genes that are targeted by each group of aberrantly retained introns. **C, D.** Boxplots displaying the distribution of percentage retention for all 349 manually curated retained introns, 237 nuclear retained introns (gold), 63 cytoplasmic and nuclear retained introns, and 49 cytoplasmic retained introns in control MNs (white boxes), FUS mutant mutant MNs (green boxes; **C**) or SOD1 mutant MNs samples (blue boxes; **D**) (Kiskinis *et al.*, 2014; Kapeli *et al.*, 2016). Mutant samples exhibit systematically a higher proportion of IR compared with controls. P-values obtained from linear mixed models accounting for idiosyncratic variations between the animals. Data shown as box plots in which the centre line is the median, limits are the interquartile range and whiskers are the minimum and maximum. **E.** Bar graphs quantifying percentage IR in SFPQ gene at DIV=0, 3, 7 and 14 in control and *VCP^{mu}* samples (mean ± s.d.; Fisher count test) in the nucleus (left) and cytoplasm (right). **F.** Bar graph showing IR levels analysed by qPCR at DIV =14 in control and *VCP^{mu}* cytosolic fractions for SFPQ and measured by normalising the levels of SFPQ IRT over the SFPQ expression level for each line. **G.** Abundance of SFPQ IRT in the cytoplasm at DIV=14 measured by qPCR and normalised over the compartment specific housekeeping genes NIT1 and NFX1. In F and G data is expressed as fold change over the control group mean; data displayed as bar plots with mean±s.d. from four lines per group, with each datapoint representing the average across two technical replicates (*p<0.05, **p<0.01, unpaired t-test).

Figure 3 Cytoplasmic intron-retaining transcripts create a mislocalization-prone environment for bound RBPs. A, B, C, D. Comparison of intron length, GC content (%), conservation scores and median enrichment for RBP binding sites of the three groups of aberrantly retained introns. Boxplots are as shown in Figures 1. **C,D**. P-values obtained from Mann-Withney test. All introns in the gene-set targeted by IR in VCP^{mu} at DIV=14 (white). **E.** Heatmap of the enrichment score of the crosslinking events in each of the 49 predominantly cytoplasmic aberrant IRTs for 27 RBPs that exhibit significantly higher enrichment compared to the two other categories of IRTs (i.e. predominantly nuclear and those that are both cytoplasmic and nuclear). **F.** Network of protein–protein interactions for 21 (out of the 27) RBPs enriched in cytoplasmic aberrant retained introns. Edges represent experimentally determined protein–protein interactions annotated in the STRING database (Szklarczyk *et al.*, 2017)**.** 9 of these RBPs belong to the *Processing of Capped Intron-Containing Pre-mRNA* Reactome(Croft *et al.*, 2014) pathway (filled magenta circles) and 3 are RBPs that exhibit hallmark nuclear-to-cytoplasmic mislocalization ALS (green circle). Line thickness indicates the strength of data support based on text mining and experiments. **G.** Comparison of enrichment across all genes within each category for SFPQ crosslinking events in the retained introns between the 3 groups of aberrantly retained introns. Boxplots are as shown in Figures 1. **C,D**. P-values obtained from Mann-Withney test. **H.** RNA immunoprecipitation (RIP) performed on the cytoplasmic lysates from control and VCP^{mu} at DIV=14 using antibodies for SFPQ or normal IgG as negative control. Levels of associated mRNA transcripts were analysed by qRT-PCR using primers designed against the indicated targets (n=4). See also Supplementary Figure 3A. **I.** Bar graphs showing qRT-PCR analysis of levels of indicated transcripts in total input of cytoplasmic lysates from DIV=14 control and VCP^{mu} samples. Values were normalised to the geometric mean of two compartment specific housekeeping genes, *NFX1* and *NIT1*, before being expressed as fold change over control group mean. (* = P<0.05 Mann-Whitney Test, *n*=4 lines per group).

Figure 4. Schematic diagram of proposed model where cytoplasmic intron-retaining transcript accumulation in ALS leads to protein mislocalization.

ACKNOWLEDGMENTS

The authors wish to thank the patients for fibroblast donations. We also thank Anob M Chakrabarti for sharing BED files of aligned CLIP data. We are grateful for the help and support provided by the Scientific Computing section and the DNA Sequencing section of Research Support Division at OIST.

FUNDING STATEMENT

This work was supported by the Idiap Research Institute and by the Francis Crick Institute which receives its core funding from Cancer Research UK (FC010110), the UK Medical Research Council (FC010110), and the Wellcome Trust (FC010110). D.M.T. is supported by a Newton-Mosharafa scholarship. R.P. holds an MRC Senior Clinical Fellowship [MR/S006591/1]. We also acknowledge Wellcome Trust funding to N.M.L.[103760/Z/14/Z], an MRC eMedLab Medical Bioinformatics Infrastructure Award to N.M.L. (MR/L016311/1). N.M.L. is a Winton Group Leader in recognition of the Winton Charitable Foundation's support towards the establishment of the Francis Crick Institute.

COMPETING INTERESTS STATEMENT

The authors report no competing interests.

REFERENCES

Boutz PL, Bhutkar A, Sharp PA. Detained introns are a novel, widespread class of post-transcriptionally spliced introns. Genes Dev 2015; 29: 63–80.

Braun CJ, Stanciu M, Boutz PL, Patterson JC, Calligaris D, Higuchi F, et al. Coordinated Splicing of Regulatory Detained Introns within Oncogenic Transcripts Creates an Exploitable Vulnerability in Malignant Glioma. Cancer Cell 2017; 32: 411–26.e11.

Braunschweig U, Barbosa-Morais NL, Pan Q, Nachman EN, Alipanahi B, Gonatopoulos-

Pournatzis T, et al. Widespread intron retention in mammals functionally tunes transcriptomes. Genome Res 2014; 24: 1774–86.

Braunschweig U, Barbosa-Morais NL, Pan Q, Nachman EN, Alipanahi B, Gonatopoulos-Pournatzis T, et al. Widespread intron retention in mammals functionally tunes transcriptomes. Genome Res 2014; 24: 1774–86.

Buckley PT, Lee MT, Sul J-Y, Miyashiro KY, Bell TJ, Fisher SA, et al. Cytoplasmic intron sequence-retaining transcripts can be dendritically targeted via ID element retrotransposons. Neuron 2011; 69: 877–84.

Colak D, Ji S-J, Porse BT, Jaffrey SR. Regulation of axon guidance by compartmentalized nonsense-mediated mRNA decay. Cell 2013; 153: 1252–65.

Croft D, Mundo AF, Haw R, Milacic M, Weiser J, Wu G, et al. The Reactome pathway knowledgebase. Nucleic Acids Res 2014; 42: D472–7.

Galante PAF, Sakabe NJ, Kirschbaum-Slager N, de Souza SJ. Detection and evaluation of intron retention events in the human transcriptome. RNA 2004; 10: 757–65.

Hall CE, Yao Z, Choi M, Tyzack GE, Serio A, Luisier R, et al. Progressive Motor Neuron Pathology and the Role of Astrocytes in a Human Stem Cell Model of VCP-Related ALS. Cell Rep 2017; 19: 1739–49.

Harley J, Hagemann C, Serio A, Patani R. FUS is lost from nuclei and gained in neurites of motor neurons in a human stem cell model of VCP-related ALS [Internet]. Brain 2020Available from: http://dx.doi.org/10.1093/brain/awaa339

Harley J, Patani R. Stress-Specific Spatiotemporal Responses of RNA-Binding Proteins in Human Stem-Cell-Derived Motor Neurons [Internet]. Int J Mol Sci 2020; 21Available from: http://dx.doi.org/10.3390/ijms21218346

Hogan AL, Grima N, Fifita JA, McCann EP, Heng B, Fat SCM, et al. SFPQ intron retention, reduced expression and aggregate formation in central nervous system tissue are pathological features of amyotrophic lateral sclerosis [Internet]. Available from: http://dx.doi.org/10.1101/2020.09.22.309062

Holt CE, Bullock SL. Subcellular mRNA localization in animal cells and why it matters. Science 2009; 326: 1212–6.

Irimia M, Weatheritt RJ, Ellis JD, Parikshak NN, Gonatopoulos-Pournatzis T, Babor M, et al. A highly conserved program of neuronal microexons is misregulated in autistic brains. Cell 2014; 159: 1511–23.

Kapeli K, Pratt GA, Vu AQ, Hutt KR, Martinez FJ, Sundararaman B, et al. Distinct and shared functions of ALS-associated proteins TDP-43, FUS and TAF15 revealed by multisystem analyses. Nat Commun 2016; 7: 12143.

Khaladkar M, Buckley PT, Lee MT, Francis C, Eghbal MM, Chuong T, et al. Subcellular RNA sequencing reveals broad presence of cytoplasmic intron-sequence retaining transcripts in mouse and rat neurons. PLoS One 2013; 8: e76194.

Kilchert C, Wittmann S, Passoni M, Shah S, Granneman S, Vasiljeva L. Regulation of mRNA Levels by Decay-Promoting Introns that Recruit the Exosome Specificity Factor Mmi1. Cell Rep 2015; 13: 2504–15.

Kiskinis E, Sandoe J, Williams LA, Boulting GL, Moccia R, Wainger BJ, et al. Pathways disrupted in human ALS motor neurons identified through genetic correction of mutant SOD1. Cell Stem Cell 2014; 14: 781–95.

Luisier R, Tyzack GE, Hall CE, Mitchell JS, Devine H, Taha DM, et al. Intron retention and nuclear loss of SFPQ are molecular hallmarks of ALS. Nat Commun 2018; 9: 2010.

Mauger O, Lemoine F, Scheiffele P. Targeted Intron Retention and Excision for Rapid Gene Regulation in Response to Neuronal Activity. Neuron 2016; 92: 1266–78.

Neumann M, Sampathu DM, Kwong LK, Truax AC, Micsenyi MC, Chou TT, et al. Ubiquitinated TDP-43 in frontotemporal lobar degeneration and amyotrophic lateral sclerosis. Science 2006; 314: 130–3.

Pervouchine D, Popov Y, Berry A, Borsari B, Frankish A, Guigó R. Integrative transcriptomic analysis suggests new autoregulatory splicing events coupled with nonsense-mediated mRNA decay. Nucleic Acids Res 2019; 47: 5293–306.

Price AJ, Hwang T, Tao R, Burke EE, Rajpurohit A, Shin JH, et al. Characterizing the nuclear and cytoplasmic transcriptomes in developing and mature human cortex uncovers new insight into psychiatric disease gene regulation. Genome Res 2020; 30: 1–11.

Saini H, Bicknell AA, Eddy SR, Moore MJ. Free circular introns with an unusual branchpoint in neuronal projections [Internet]. Elife 2019; 8Available from: http://dx.doi.org/10.7554/eLife.47809

Sakabe NJ, de Souza SJ. Sequence features responsible for intron retention in human. BMC Genomics 2007; 8: 59.

Sharangdhar T, Sugimoto Y, Heraud-Farlow J, Fernández-Moya SM, Ehses J, de los Mozos IR, et al. A retained intron in the 3′- UTR of Calm3 mRNA mediates its Staufen2- and activity-dependent localization to neuronal dendrites. EMBO reports 2017; 18: 1762–74.

Sloan CA, Chan ET, Davidson JM, Malladi VS, Strattan JS, Hitz BC, et al. ENCODE data at the ENCODE portal. Nucleic Acids Res 2016; 44: D726–32.

Sreedharan J, Blair IP, Tripathi VB, Hu X, Vance C, Rogelj B, et al. TDP-43 mutations in familial and sporadic amyotrophic lateral sclerosis. Science 2008; 319: 1668–72.

Stagsted LVW, O'Leary ET, Hansen TB. The RNA-binding protein SFPQ preserves long-intron splicing and regulates circRNA biogenesis [Internet]. Available from: http://dx.doi.org/10.1101/2020.09.04.280750

Szklarczyk D, Morris JH, Cook H, Kuhn M, Wyder S, Simonovic M, et al. The STRING database in 2017: quality-controlled protein-protein association networks, made broadly accessible. Nucleic Acids Res 2017; 45: D362–8.

Tyzack GE, Luisier R, Taha DM, Neeves J, Modic M, Mitchell JS, et al. Widespread FUS

mislocalization is a molecular hallmark of amyotrophic lateral sclerosis. Brain 2019; 142: 2572–80.

Vance C, Rogelj B, Hortobagyi T, De Vos KJ, Nishimura AL, Sreedharan J, et al. Mutations in FUS, an RNA Processing Protein, Cause Familial Amyotrophic Lateral Sclerosis Type 6. Science 2009; 323: 1208–11.

Van Nostrand EL, Freese P, Pratt GA, Wang X, Wei X. A large-scale binding and functional map of human RNA binding proteins [Internet]. bioRxiv 2017Available from: https://www.biorxiv.org/content/early/2017/08/23/179648.abstract

Wong JJ-L, Ritchie W, Ebner OA, Selbach M, Wong JWH, Huang Y, et al. Orchestrated intron retention regulates normal granulocyte differentiation. Cell 2013; 154: 583–95.

Yap K, Lim ZQ, Khandelia P, Friedman B, Makeyev EV. Coordinated regulation of neuronal mRNA steady-state levels through developmentally controlled intron retention. Genes Dev 2012; 26: 1209–23.

Yap K, Lim ZQ, Khandelia P, Friedman B, Makeyev EV. Coordinated regulation of neuronal mRNA steady-state levels through developmentally controlled intron retention. Genes Dev 2012; 26: 1209–23.

Figure 1

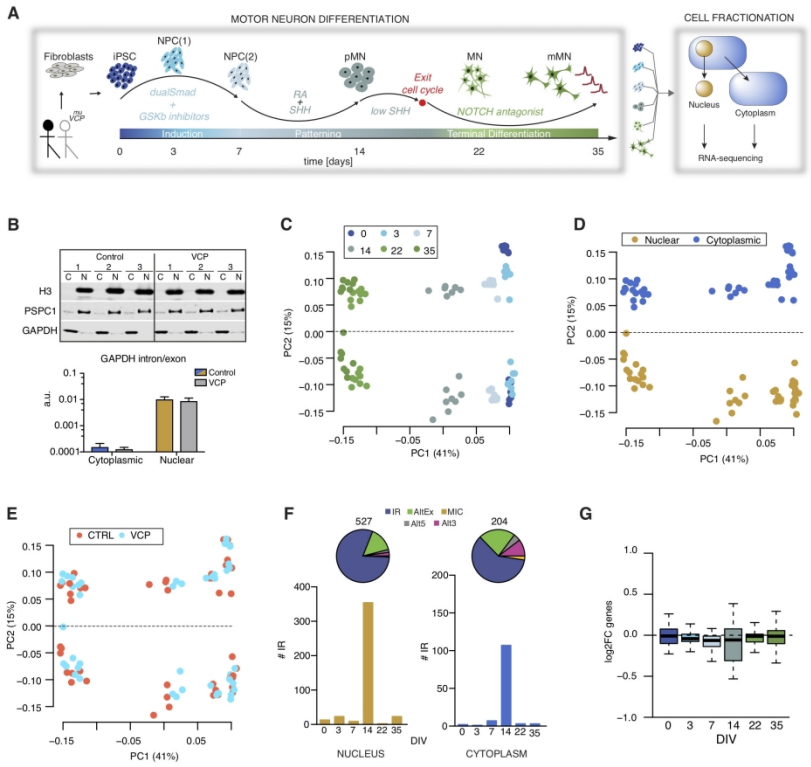

Figure 1 | Time-resolved cellular fractionation and RNA-sequencing during human motor neurogenesis reveals widespread aberrant cytoplasmic IR in ALS. A. Schematic depicting the iPSC differentiation strategy for motor neurogenesis. Arrows indicate sampling time-points in days when cells were fractionated into nuclear and cytoplasmic compartments prior to deep (polyA) RNA-sequencing. Four iPSC clones were obtained from four different healthy controls and three iPSC clones from two ALS patients with VCP mutations: R155C and R191Q; hereafter termed VCPmu. Induced-pluripotent stem cells (iPSC); neural precursors (NPC); "patterned" precursor motor neurons (ventral spinal cord; pMN); post-mitotic but electrophysiologically inactive motor neurons (MN); electrophysiologically active MNs (mMN). B. Representative QC data for fractionation of samples at DIV=14 at protein level (Western blot, top) and RNA level (qPCR, bottom). In the Western blot, histone H3 and PSPC1 were chosen as protein markers for the nuclear faction, and GAPDH was used as cytosolic marker. In the qPCR, the ratio between intronic and exonic GAPDH sequences was measured in both fractions to exclude the leakage of nuclear RNA into the cytosolic fraction due to disruption of nuclei during the fractionation. Data is expressed as mean±SD from four lines per group. C. SVD performed on normalized 18,834 gene expression values across 95 samples.

Samples are plotted by their coordinates along PC1 (41% of variance) and PC2 (15% of variance). Colors of data points indicate similar time in culture: iPSC (dark blue), DIV=3 (blue; NPC1), DIV=7 (light blue; NPC2), DIV=14 (grey; pMN), DIV=22 (lightgreen; MN) and DIV=35 (dark green; eMN). D. Same as (C) with colors of data points indicating similar cellular fractions: nuclear fraction (gold) and cytoplasmic fraction (blue). E. Same as (C) with colors of data points indicating either control samples (red) or VCPmu samples (blue). F. (upper) Pie charts representing proportions of included splicing events in VCPmu at all timepoints of motor neurogenesis compared with age-matched control samples in nuclear (upper chart) and cytoplasmic (lower chart) fractions. Total number of events are indicated above the chart. Intron retention (IR); alternative exon (AltEx); microexons (MIC); alternative 5' and 3' UTR (Alt5 and Alt3). (lower) Bar graphs representing the number of retained introns in VCPmu compared to control samples at specific timepoints during MN differentiation. Nuclear fraction (gold; left). Cytoplasmic fraction (blue; right). G. Boxplots showing the distributions of cytoplasmic log2 fold-changes for 72 essential splicing factor genes (Table S8) between VCPmu and controls.

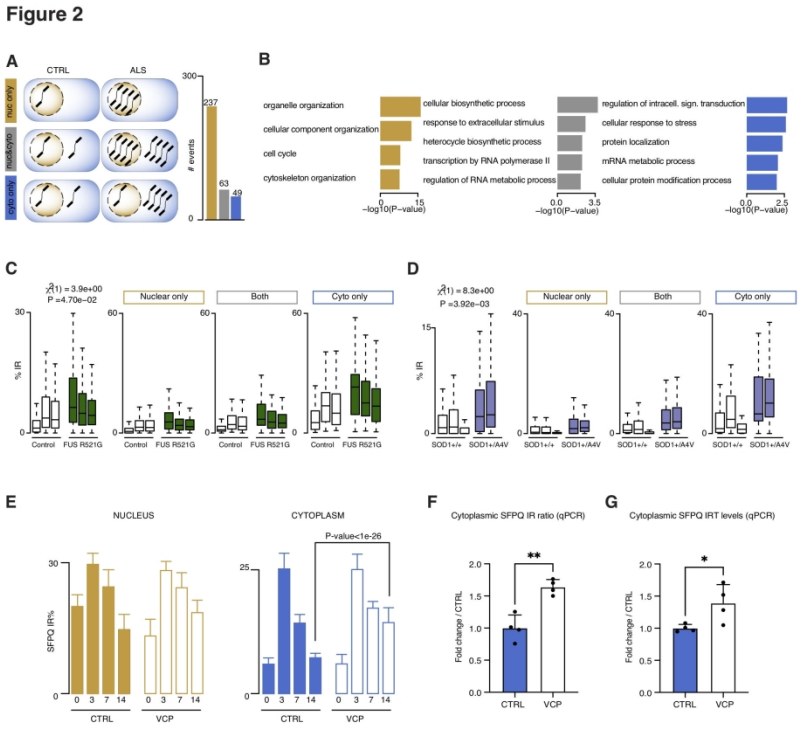

Figure 2 | Aberrant nuclear and cytoplasmic intronic sequences exhibit distinct characteristics. A. Schematic of our proposed taxonomy for aberrant IRTs (left) and bar graphs (right) representing the numbers of retained introns in VCPmu compared to control samples at DIV=14 that are predominantly nuclear (gold bar), aberrant in both nucleus and cytoplasm (grey bar), or predominant in cytoplasm (blue bar). The number of events in each category is indicated above the bar. B. Bar plots displaying the enrichment scores for GO biological functions of genes that are targeted by each group of aberrantly retained introns. C, D. Boxplots displaying the distribution of percentage retention for all 349 manually curated retained introns, 237 nuclear retained introns (gold), 63 cytoplasmic and nuclear retained introns, and 49 cytoplasmic retained introns in control MNs (white boxes), FUS mutant mutant MNs (green boxes; C) or SOD1 mutant MNs samples (blue boxes; D) (Kiskinis et al., 2014; Kapeli et al., 2016). Mutant samples exhibit systematically a higher proportion of IR compared with controls. P-values obtained from linear mixed models accounting for idiosyncratic variations between the animals. Data shown as box plots in which the centre line is the median, limits are the interquartile range and whiskers are the minimum and maximum. E. Bar graphs quantifying percentage IR in SFPQ gene at DIV=0, 3, 7 and 14 in control and VCPmu samples (mean ± s.d.;

Fisher count test) in the nucleus (left) and cytoplasm (right). F. Bar graph showing IR levels analysed by qPCR at DIV =14 in control and VCPmu cytosolic fractions for SFPQ and measured by normalising the levels of SFPQ IRT over the SFPQ expression level for each line. G. Abundance of SFPQ IRT in the cytoplasm at DIV=14 measured by qPCR and normalised over the compartment specific housekeeping genes NIT1 and NFX1. In F and G data is expressed as fold change over the control group mean; data displayed as bar plots with mean±s.d. from four lines per group, with each datapoint representing the average across two technical replicates (*p<0.05, **p<0.01, unpaired t-test).

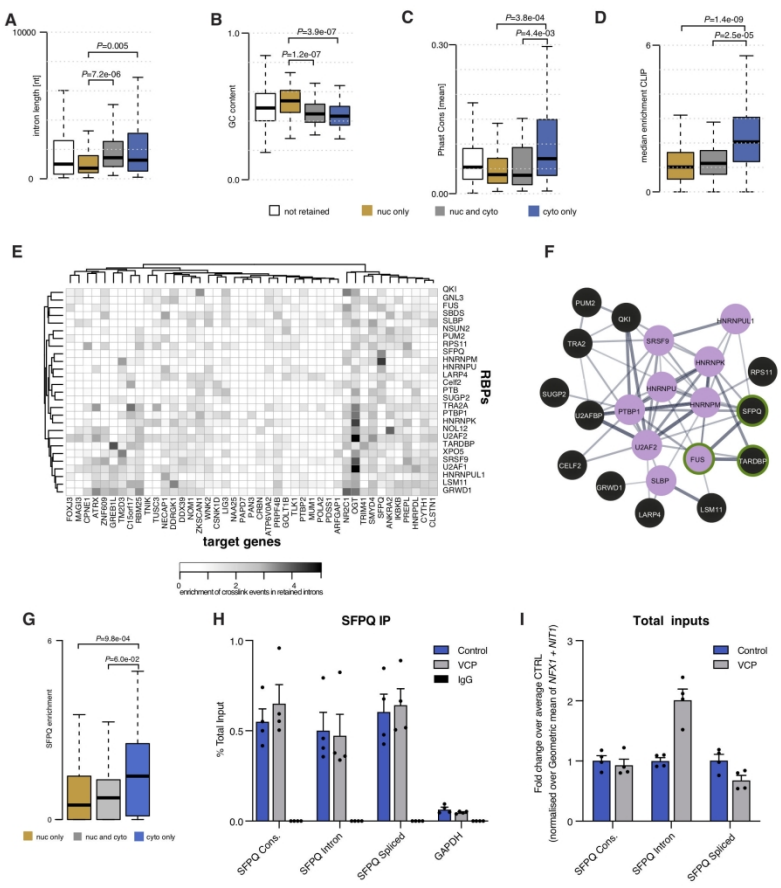

Figure 3 | Cytoplasmic intron-retaining transcripts create a mislocalization-prone environment for bound RBPs. A, B, C, D. Comparison of intron length, GC content (%), conservation scores and median enrichment for RBP binding sites of the three groups of aberrantly retained introns. Boxplots are as shown in Figures 1. C,D. P-values obtained from Mann-Withney test. All introns in the gene-set targeted by IR in VCPmu at DIV=14 (white). E. Heatmap of the enrichment score of the crosslinking events in each of the 49 predominantly cytoplasmic aberrant IRTs for 27 RBPs that exhibit significantly higher enrichment compared to the two other categories of IRTs (i.e. predominantly nuclear and those that are both cytoplasmic and nuclear). F. Network of protein–protein interactions for 21 (out of the 27) RBPs enriched in cytoplasmic aberrant retained introns. Edges represent experimentally determined protein–protein interactions annotated in the STRING database (Szklarczyk et al., 2017). 9 of these RBPs belong to the Processing of Capped Intron-Containing Pre-mRNA Reactome(Croft et al., 2014) pathway (filled magenta circles) and 3 are RBPs that exhibit hallmark nuclear-to-cytoplasmic mislocalization ALS (green circle). Line thickness indicates the strength of data support based on text mining and experiments. G. Comparison of enrichment across all genes within each category for SFPQ crosslinking events in the retained introns between the 3

groups of aberrantly retained introns. Boxplots are as shown in Figures 1. C,D. P-values obtained from Mann-Withney test. H. RNA immunoprecipitation (RIP) performed on the cytoplasmic lysates from control and VCPmu at DIV=14 using antibodies for SFPQ or normal IgG as negative control. Levels of associated mRNA transcripts were analysed by qRT-PCR using primers designed against the indicated targets (n=4). See also Supplementary Figure 3A. I. Bar graphs showing qRT-PCR analysis of levels of indicated transcripts in total input of cytoplasmic lysates from DIV=14 control and VCPmu samples. Values were normalised to the geometric mean of two compartment specific housekeeping genes, NFX1 and NIT1, before being expressed as fold change over control group mean. (* = P<0.05 Mann-Whitney Test, n=4 lines per group).

Figure 4

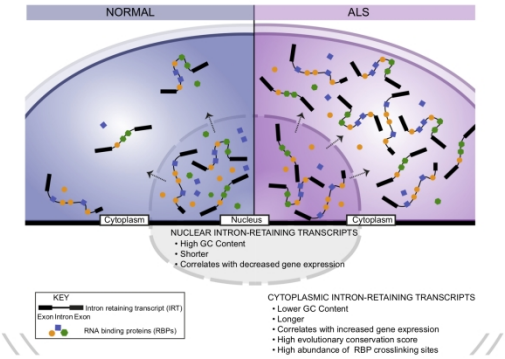

Figure 4. Schematic diagram of proposed model where cytoplasmic intron-retaining transcript accumulation in ALS leads to protein mislocalization.

202x296mm (300 x 300 DPI)